A numerical investigation of the sliding contact between a rigid spherical indenter and a rubber surface: The effect of sliding depth and surface roughness

Budi Setiyana [1,2*], Jamari Jamari [1], Rifky Ismail [1], Dirk Jan Schipper [2]

[1] Engineering Design and Tribology Laboratory, Mechanical Engineering Department, University of Diponegoro, INDONESIA.
[2] Laboratory for Surface Technology and Tribology, Faculty of Engineering Technology, University of Twente, NETHERLANDS.
*Corresponding author: bsetiyana@yahoo.com

KEYWORDS	ABSTRACT
Adhesion Deformation Friction Roughness	Sliding analysis of the rubber with respect to friction is important especially related to the braking capacity of a tyre rubber. The friction force of the contact between a rubber surface and its counter-face is often caused as a combination of deformation and adhesion (roughness) effects. Due to the non-linear behaviour of the rubber material, friction phenomenon on the rubber is difficult to analyse theoretically; therefore, a numerical method is often applied. This paper discusses the phenomenon of friction between a rubber surface (SBR-25) and a rigid spherical indenter. The analysis was carried out numerically using FE Analysis with a specified sliding velocity of the indenter. The rubber used is commonly applied as tyre material and modelled as a hyper-elastic material. Friction contact phenomena were observed based on variations in sliding depth and surface roughness. The results obtained were stress distribution, maximum stress, contact forces and coefficient of friction. In general, the results showed that a dynamic phenomenon emerged at a great sliding depth and high surface roughness. This is indicated by fluctuating values of the stress, contact forces and friction coefficient during sliding.

1.0   INTRODUCTION

Rubber is commonly applied in equipment in which the rubber components experience friction. It is important to analyse the frictional contact by evaluating the resistance force, braking capacity of the tyre rubber and abrasion wear resistance of the rubber surface. Moreover, a dynamic phenomenon may occur in the form of stick-slip, resulting in fluctuating contact forces due to elastic and compliant behaviour of the rubber (Maegawa et al., 2006; Uchiyama and Ishino, 1992; Fukahori and Yamazaki, 1995; Khafidh et al., 2018). Due to the dynamic phenomenon a periodic wear pattern is shown on the abraded rubber surface (Fukahori and Yamazaki, 1994; Setiyana et al., 2018; Fukahori and Yamazaki, 1994; Coveney and Menger, 1999). This phenomenon can generally be seen on the surface of seals, tyres and transmission belts that have been abraded. The coefficient of friction is an associated important parameter, which is obtained by comparing the tangential and normal force. As commonly defined, the coefficient of friction is influenced by surface roughness (adhesion component) and deformation (hysteresis component) during sliding processes (Gent, 1992; Zhang, 2004). In general, surface roughness is easy to be determined; whereas the deformation effect is very difficult to be determined theoretically. Therefore, a numerical method is usually applied (Palfi et al., 2015; Soos and Gooda, 2007; Podra and Andersson, 1999). However, the dynamic phenomenon of the rubber during friction is still less attention, which might be influenced by the degree of deformation and surface roughness.

Rubber has unique properties and is often modelled as a hyper-elastic material. Due to its non-linear properties, rubber behaviour is difficult to analyse. Tensile testing shows that rubber is very elastic and has small hysteresis effects (Gent, 1992). Thus, in many cases, the hysteresis cycle of the stress-strain relationship can be averaged and represented by a single line. This single line of the stress-strain relationship is known as the hyper-elastic line and is commonly used to represent the rubber material properties in numerical analysis (MSC Software Whitepaper, 2010).

This study investigates the friction between Styrene Butadiene Rubber, filled with a weight of 25% carbon black (SBR-25), and a rigid spherical indenter. The analysis was performed using a numerical method based on Finite Element Analysis (FEA) with a specified sliding velocity of the indenter. Numerical simulation was carried out to investigate the effects of the sliding depths (which represents the deformation degree) and surface roughness (which represents the adhesion degree) on sliding contact phenomena. In this study, the adhesion term is in macroscopic view that states the roughness degree of the contact surface between the indenter and the rubber. The simulation results in this study are presented graphically to discuss parameters such as maximum stress, contact force and coefficient of friction.

2.0   METHODS

This work was carried out numerically using a commercial software package, ABAQUS 6.11 (ABAQUS 6.11., 2011). Stress-strain data from a tensile test is required for the FE simulation for modelling the rubber as a hyper-elastic material. This study used rubber SBR-25 (Styrene Butadiene Rubber with 25% weight of carbon black). Carbon black was incorporated into the compound to modify the stiffness of the SBR compound, which is widely encountered in tyre tread applications. The formulation of the compound used is given in Table 1.

In FE simulation input, the rubber was modelled as a hyper-elastic and incompressible material, moreover, its mechanical properties were stated as a Strain Energy Function (SEF). There are several types of SEF proposed by some experts depending on the rubber material properties. The SEF used for the SBR-25 was Yeoh type and adopted from Liang's analysis (Liang,

2007). Analysis to obtain the SEF coefficient was performed from stress-strain curve that obtained experimentally by a uniaxial tensile test. The stress-strain curve is typically presented in Figure 1 in the form of engineering stress σ vs extension ratio λ. It has been noted that the extension ratio is the ratio between final length and initial length of the rubber specimen along tensile test. As a comparison, if the rubber is modelled as an elastic linear material, the stress-strain linearization provides an elastic modulus around of 2.87 MPa.

Table 1: Formulations for the rubber materials (part per hundred rubber/phr).

Ingredients	SBR-25
Styrene Butadiene Rubber	100
Carbon Black	25
Zinc Oxide	3.0
Stearic acid	1.0
Sulphur	3.0
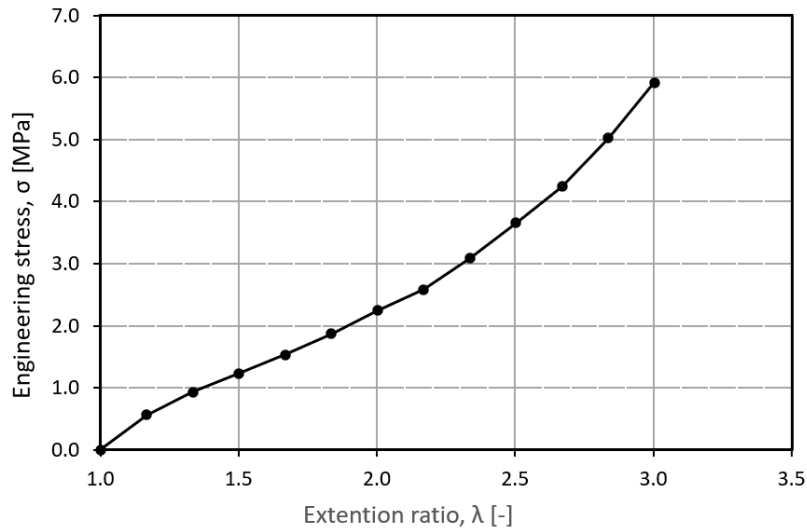
Figure 1: Engineering stress vs Extension ratio diagram for SBR-25.

Based on Figure 1, the coefficients of SEF i.e. C_{10}, C_{20} and C_{30} were obtained using Equation (1), Equation (2) and Equation (3) as following (Yeoh, 1990),

$$\frac{\sigma^*}{2} = 3C_{30}(I_1 - 3)^2 + 2C_{20}(I_1 - 3) + C_{10} \tag{1}$$

$$\sigma^* = \frac{\sigma}{(\lambda - \lambda^{-2})} \tag{2}$$

$$I_1 = \lambda_1^2 + \lambda_2^2 + \lambda_3^2 \tag{3}$$

It was defined that σ^* is a reduced stress, I_1 is a strain invariant and λ_1 is extension ratio in main principal coordinate, moreover, λ_2 and λ_3 are extension ratio in others principal coordinate.

However, tensile test in the filled rubber as in SBR-25 showed that λ_2 and λ_3 are too small therefore the strain invariant I_1 only depends on λ_1 (Gregory, 1979). Using the above formulation, the obtained SEF coefficients were C_{10}=0.337MPa, C_{20}=-0.0053MPa and C_{30}=0.0005MPa. Others input data were also required i.e., a bulk compliance of the rubber (0.062 MPa^{-1}) and density (1.12x10^3 kgm^{-3}) (Liang, 2007).

(a)

(b)
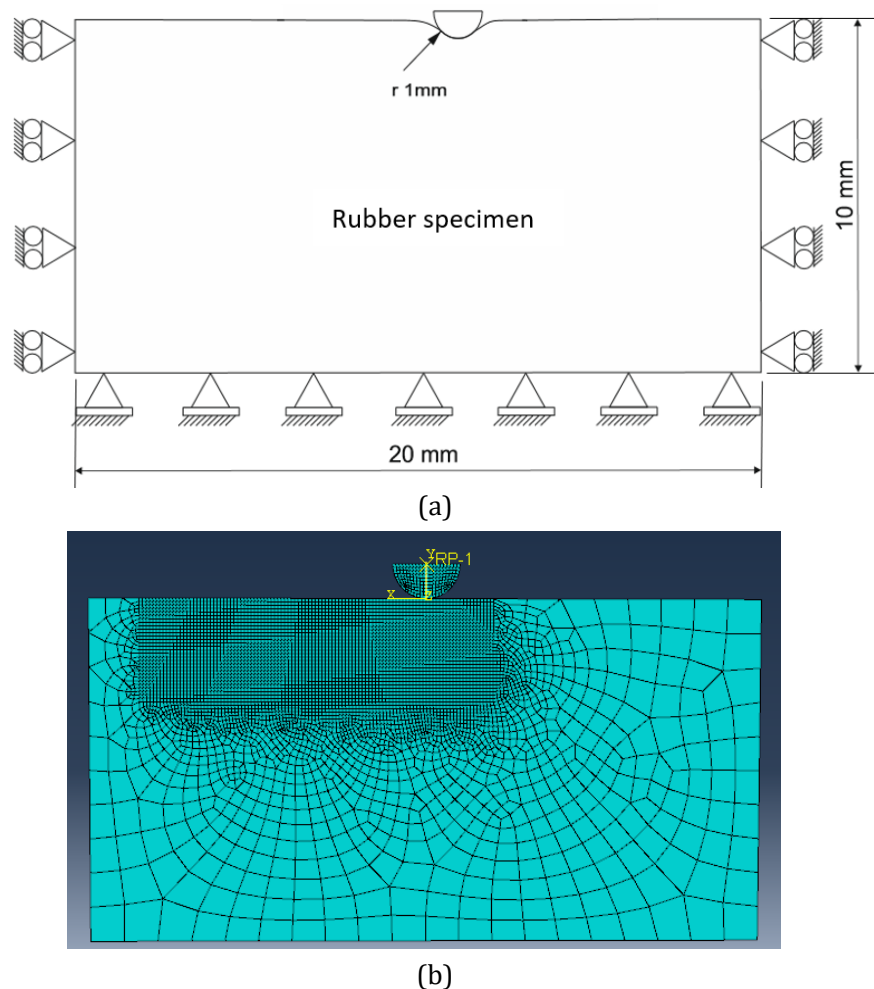
Figure 2: Rigid indenter sliding on rubber (a) Schematic model (b) FE model.

A schematic illustration of the sliding between a rigid spherical indenter and the rubber surface is shown in Figure 2(a). It may a simplification model of a small gravel in a sliding contact with the tyre rubber surface. The spherical indenter used has a 1.0 mm tip radius and the boundary conditions of the indentation system are shown in this picture as well. This analysis used model rubber specimens of 10 mm high, 20 mm wide and 10 mm thick. FE simulations of the sliding contact were carried out at a constant sliding velocity of 5 mm/s and 7.0 mm maximum sliding displacement with varying sliding depth and surface roughness. The low sliding velocity

of 5 mm/s was selected in order to avoid the high normal oscillation effect of the rubber surface along sliding (Setiyana et al., 2018).

In FE simulation input, the sliding depths selected were 0.4, 0.7 and 1.0 mm, while the surface roughness that represented by coefficients of adhesion were 0.15, 0.50 and 1.0. The sliding depth is closely related to the indenter load, therefore for simplicity, the basis of selection from the sliding depth values was that the maximum value does not extend beyond the indenter radius i.e. 1.0 mm, meanwhile the difference among those values is made the same i.e 0.3 mm. The coefficient of adhesion μ_{adh} is the same as the coefficient of kinetic friction in classical Newton's friction law. In general, the adhesion coefficient between a small gravel and tire rubber is around of 0.5, however, in order to understand the roughness effects, this study evaluated a case for extreme slippery conditions (contact between a smooth gravel and smooth virgin rubber surface, μ_{adh} was made around of 0.15) and extreme rough condition (contact between a coarse gravel and abraded or worn rubber surface, μ_{adh} was made around of 1.0). Related to the sliding depth and surface roughness, total tangential force F_t during sliding is consisting of a deformation force F_{def} (due to the sliding depth) and an adhesion force F_{adh} (due to the roughness surface) as presented in Equation (4) (Gent, 1992). Moreover, the adhesion force F_{adh} is depending on the adhesion coefficient μ_{adh} and normal force F_n as given in Equation (5).

$$F_t = F_{def} + F_{adh} \tag{4}$$

$$F_{adh} = \mu_{adh} F_n \tag{5}$$

Figure 2(b) shows the FE meshing using 3D Solid elements in order to show the surface deformation and stress distribution of the rubber around the indenter. Along contact against the rubber surface, the indenter was assumed as a perfectly rigid material and no deformation on it. A fine mesh of the rubber material was applied around the sliding contact area using 3D brick or hexahedra elements in order to obtain accurate results of the FE simulations (MSC Software Whitepaper, 2010). FE meshing analysis was also performed to find the suitable number or size of those elements in order to obtain the convergence results of FE output. Validation was performed to find the element size around the indenter tip in extreme condition i. e. maximum stress resulted for high sliding depth and surface roughness. Convergence analysis was stopped if the stress change were less significant to the element size reduction process. The number of elements used in this FE simulation is 5680.

The FE simulation was evaluated in three steps of the indenter movement: the start or 'rest' position (initial state), followed by the 'moving' condition (sliding state) and finally the 'stop' condition (final state). The FEA outputs were presented in the form of stress patterns and deformation contours. From these results, the maximum stress and its location were determined. Finally, the maximum stress was plotted graphically concerning the various input data. In addition to the results of the stress, the tangential force, normal force and coefficient of friction were also presented as a function of sliding depth and surface roughness. Based on the simulations output, it can be determined which results indicate dynamic phenomena.

3.0   RESULTS AND DISCUSSION

Figure 3 shows the FEA output of the von Mises stress field of the SBR-25 as well as the deformation contours of the surface by the sliding sphere. The FEA outputs with 1.0 mm sliding indentation depth and 0.15 for the coefficient of adhesion are presented in this figure, starting from (a) the initial state, (b) the sliding state and (c) the final state. The legend shows the von Mises stress occurring at the final state. During the simulation, the area with highest contact stress was located below the tip of the indenter. In the initial state, the stress distribution was symmetrical because it was still in a static contact. For the sliding state, the shape of the stress field became asymmetrical and in the final state the shape of the stress field was similar to the sliding state. Furthermore, for the sliding and final states, the maximum stress was located mostly at the rear of the indenter. A three-dimensional presentation of the stress distribution is shown in Figure 4 for the sliding state with 1.033 MPa maximum stress.
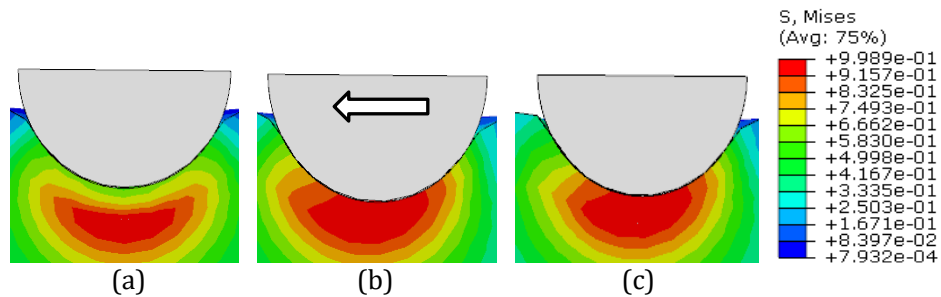
Figure 3: The stress distribution in 2 dimensions section of the rubber for 1.0 mm sliding depth and 0.15 adhesion COF (a) Initial state (b) Sliding state (c) Final state.
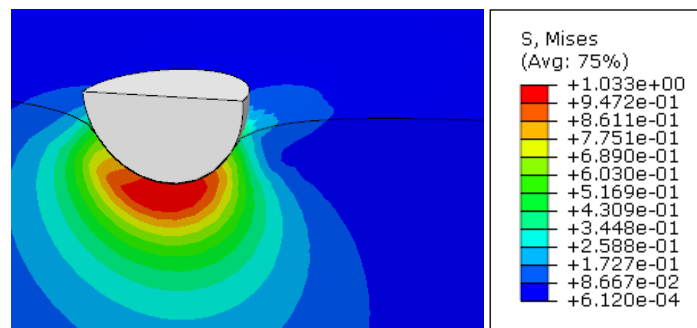
Figure 4: The rubber stress field in 3 dimensions section in the sliding state.

The maximum stress that occurs during the sliding process is shown in Figure 5 and Figure 6. The maximum stresses data are given for different sliding depths and values of the adhesion coefficient. With 0.5 as adhesion coefficient, it is shown that a greater sliding depth led to a greater maximum stress and fluctuating values are also shown, as seen in Figure 5. Besides, a fluctuating maximum stress also occurred when the value of the adhesion coefficient (surface roughness) was large. Figure 6 shows that for a 0.7 mm indentation depth and 1.0, adhesion coefficient also provided a fluctuating stress. In general, it can be concluded that the dynamic phenomena occur when the sliding indentation is carried out for a great sliding depth and high coefficient of adhesion. In the rubber abrasion test, the fluctuating maximum stress may produce discrete and

periodic surface cracks which eventually form a periodic wear pattern at the abraded rubber surface. This, along with the mechanism, is as presented in (Khafidh et al., 2018).
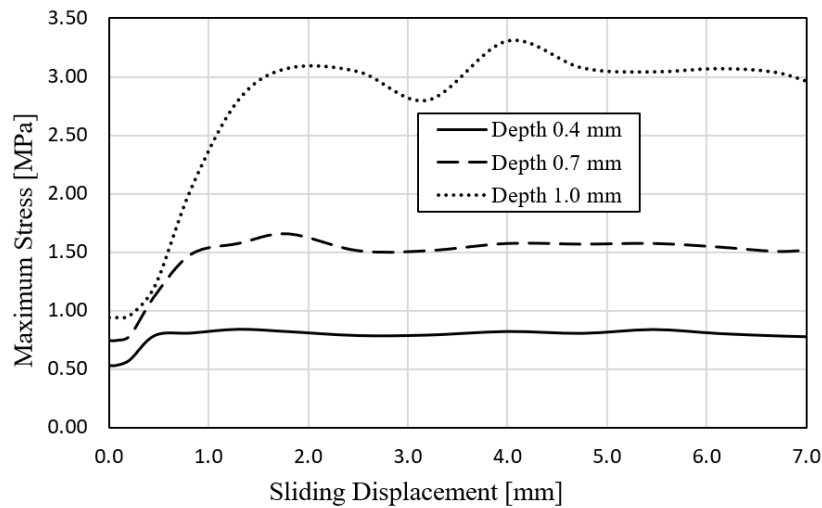
Figure 5: The maximum stress for various sliding depths, adhesion coefficient is 0.5.
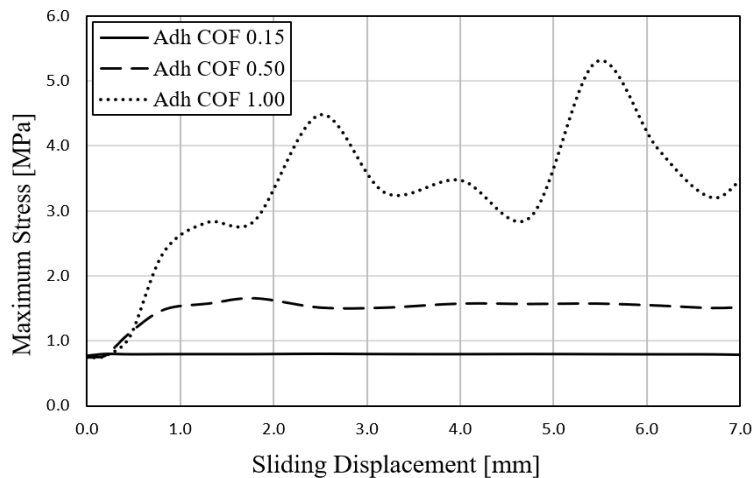
Figure 6: The maximum stress for various surface roughness values (adhesion coefficient), sliding depth is 0.7 mm.

The calculated contact forces are shown in Figure 7 for 0.4 mm, 0.7 mm and 1.0 mm indentation depth. The contact forces were calculated by adding up all the reaction forces from the nodes at the rubber material supports in normal as well as tangential direction. Simulations were carried out for a 1.0 adhesion coefficient, which may represent a rough indenter and rubber surface i.e. an abraded or worn surface. The tangential force in the sliding contact is illustrated in Figure 7(a). It shows that a great sliding depth leads to a large fluctuating tangential force. This case can be related to the stick-slip phenomenon, which commonly occurs in rubber friction

(Setiyana et al., 2016). This reflects the fact that the rubber surface oscillates in tangential direction i.e. the sliding direction of the indenter. Figure 7(b) shows the normal force, demonstrating that great sliding depths also provide increased normal forces, resulting in an oscillation of the normal force and thereby indicating a normal oscillation of the rubber surface. The inclusion of the results of other values of adhesion coefficient and sliding depth in Figure 7 will assert the conclusion that the dynamic phenomena occur when the sliding indentation is carried out for a great sliding depth and high coefficient of adhesion. This is also applicable to Figure 5 and Figure 6.

(a)

(b)
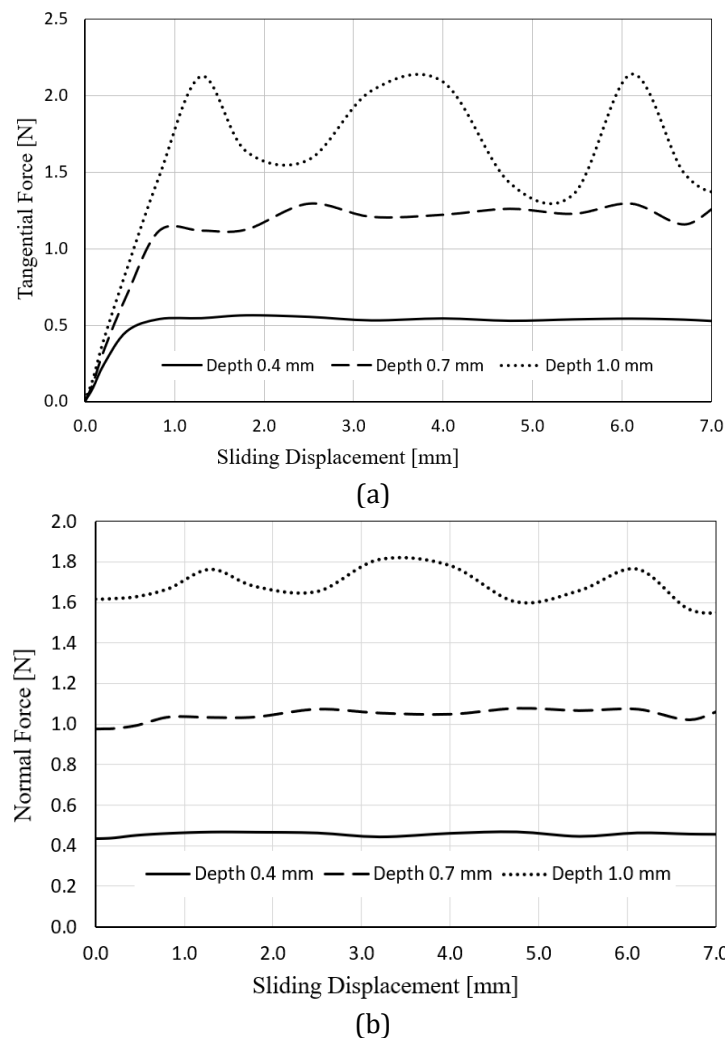
Figure 7: Contact forces for various sliding depths, adhesion coefficient is 1.0 (a) Tangential force (b) Normal force.

Sliding contact between a rigid counter surface in a contact with the rubber surface was performed experimentally in the fixed sliding depth (Coveney and Menger, 1999). Using a rigid

blade indenter as a counter surface, a high fluctuation of the tangential force was observed for a high indenter load while the normal force did not fluctuate much. Friction on a rough surface, i.e. an abraded surface also provides a very fluctuating tangential force. Qualitatively, this phenomenon is similar to the results presented in Figure 7.

(a)

(b)
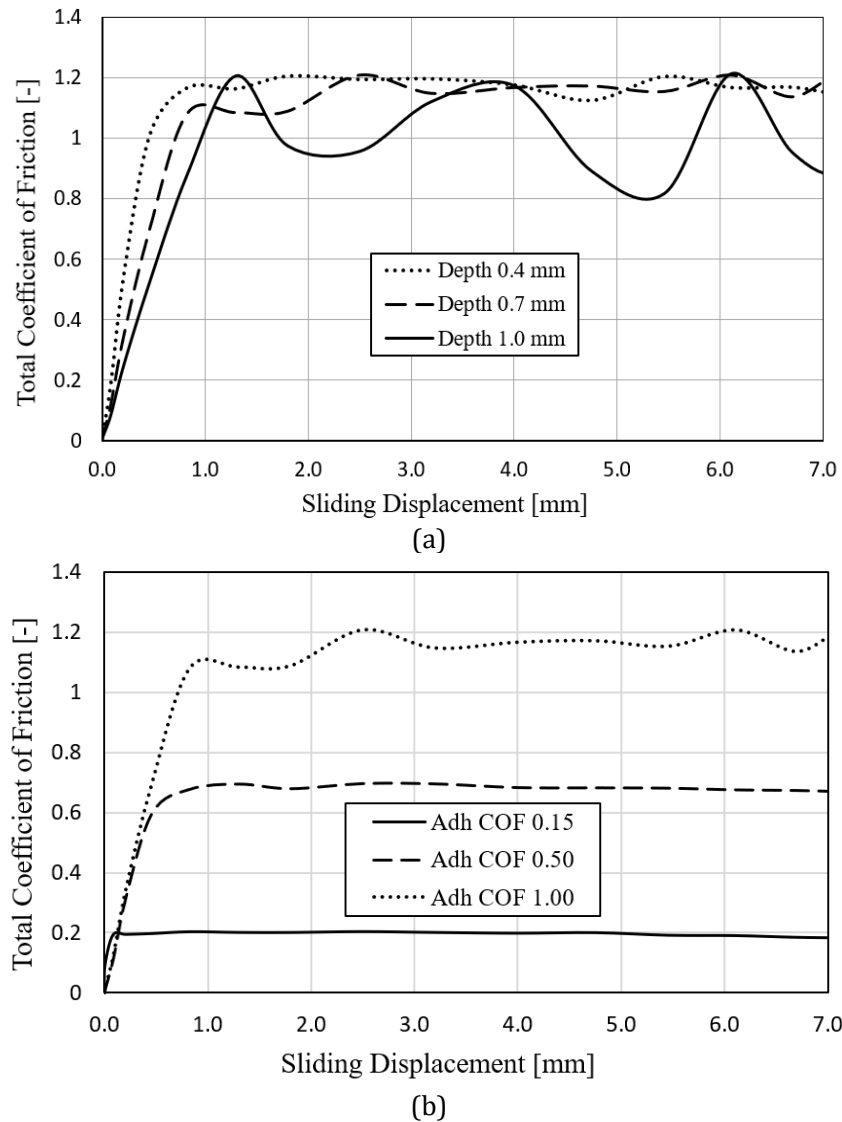
Figure 8: Coefficient of friction for rubber sliding (a) Varying the sliding depth and an adhesion coefficient of 0.5 (b) Various adhesion coefficients with a sliding depth of 0.7 mm.

The coefficient of friction (COF) as a function of the sliding distance is presented in Figure 8. The COF were obtained by dividing the tangential contact force with the normal contact force which are discussed previously. This paper simply selects the middle value of the surface roughness for various sliding depth and the middle value of the sliding depth for various surface

roughness. Figure 8(a) represents the simulation data for sliding with different depths, while Figure 8(b) is obtained for different surface roughness values (adhesion coefficient). Figure 8(a) shows that the dynamic friction coefficient occur for great sliding depths, resulting in a fluctuating coefficient of friction for adhesion coefficient of 0.5. On the other hand, the coefficient of friction for different surface roughness values shows that a greater degree of surface roughness may lead to dynamic effects. The average value of the coefficient of friction tends to decrease for great sliding depths. Qualitatively this is in accordance with the results obtained from the frictional contact between a rubber pin and a rigid glass plate (Tuononen, 2014). It also can be seen that the dynamic friction coefficient is greater if the indenter load is large. Qualitatively this is in accordance with the results of research conducted on the contact between tires and compacted asphalt (Yu et al., 2020). The dynamic friction coefficient also different for different compacted asphalt materials due to differences in surface roughness.

Based on the analysis, it can be seen that dynamic phenomena may occur in the frictional contact rubber-rigid indenter. Such phenomena occur in the form of fluctuating values of stress, contact forces and coefficient of friction. Dynamic phenomena are evident for friction contacts with great indentation depths and a high degree of surface roughness. At some specified moments along the sliding track, stick occurs due to a great indentation depth and a high degree of surface roughness. The surface of the rubber also oscillates both in tangential and normal direction. As a result, the indenter that slides relative to the rubber surface causes the stick-slip to contact to occur sequentially.

CONCLUSION

This paper discusses the effects of sliding depth and contact surface roughness on the sliding contact phenomena of rubber surfaces in contact with a spherical tip. The rubber analysed is filled Styrene Butadiene Rubber (SBR-25) which is commonly used for tyres. The analysis was carried out with a specific sliding velocity. The analysis was numerically conducted to find out the stress, contact forces and friction coefficient of the sliding contact. The simulation results show that the stress, contact force and coefficient of friction may fluctuate during sliding, especially for great indentation depths and a high degree of surface roughness. This phenomenon may be related to stick-slip contact, which is a common phenomenon occurring in rubber friction. The surface of the rubber undergoes oscillations along sliding, both in tangential and normal direction. Therefore, in rubber abrasion testing, dynamic phenomena are indicated by the periodic wear pattern of the abraded rubber surface.

REFERENCES

ABAQUS 6.11. (2011). Standard User's Manual, Dassault Systems Simulia Corp., USA.
Coveney, C. & Menger, C. (1999). Initiation and development of wear of an elastomeric surface by a blade abrader. Wear 233-235, 702-711.
Fukahori, Y. & Yamazaki, H. (1994). Mechanism of rubber abrasion—Part 2: General rule in abrasion pattern formation in rubber-like materials. Wear, 178, 109-116.
Fukahori, Y. & Yamazaki, H. (1994). Mechanism of rubber abrasion—Part 1: abrasion pattern formation in natural rubber vulcanizate. Wear, 171, 195-202.
Fukahori, Y. & Yamazaki, H. (1995). Mechanism of rubber abrasion—Part 3: how is friction linked to fracture in rubber abrasion? Wear, 188, 19-26.

Gent, A.N. (1992). Engineering with Rubber, How to design rubber components, 3rd edition, Hanser Publication, Cincinnati, USA.

Gregory, M.J. (1979). The stress / strain behaviour of filled rubbers at moderate strains. Plastics and Rubber: Materials and Applications, 4, 184-188.

Khafidh, M., Setiyana, B., Jamari, J., Masen., M.A. & Schipper, D.J. (2018). Understanding the occurrence of wavy track of elastomeric material. Wear, 412-413, 23-29.

Liang, H. (2007). Investigating the mechanism of elastomer abrasion, Doctoral Thesis, University of London, London.

Maegawa, S., Itoigawa, F. & Nakamura, T. (2006). Dynamics in sliding friction of soft adhesive elastomer: Schallamach waves as a stress-relaxation mechanism. Tribology International, 96, 23-30.

MSC Software Whitepaper. (2010). Nonlinear Finite Element Analysis of Elastomer, MSC Software Corporation, Santa Ana, USA.

Palfi, L., Goda, T., Varadi, K., Garbayo, E., Bielsa, J.M. & Jiménez, M.A. (2015). FE prediction of hysteretic component of rubber friction. Advances in Tribology, 2012, 2-13.

Podra, P. & Andersson, S. (1999). Simulating sliding wear with finite element method. Tribology International 32, 71-81.

Setiyana, B., Ismail, R., Jamari, J. & Schipper, D.J. (2016). Stick-slip behaviour of a viscoelastic flat sliding against a rigid indenter. Tribology Online, 11,3, 512-518.

Setiyana, B., Ismail, R., Jamari, J. & Schipper, D.J. (2018). Analytical study of the wear pattern of an abraded rubber surface: Interaction model. Tribology, Material Surface and Interfaces, 12(4), 186-192.

Soos, E. & Gooda, T. (2007). Numerical analysis of sliding friction rubber behaviour. Trans Tech Publication, 537-538, 615-622.

Tuononen, A.J. (2014). Digital image correlation to analyse stick–slip behaviour of tyre tread block. Tribology International, l69, 70-76.

Uchiyama, Y. & Ishino, Y. (1992). Pattern abrasion mechanism of rubber. Wear, 158, 141-155.

Yeoh, O.H. (1990). Characterisation of Elastic Properties of Carbon Black Filled Rubber Vulcanizates. Rubber chemistry and technology, 63, 792-805.

Yu, M., Xiao, B., You, Z., Wu, G., Li, X., Ding, Y. (2020). Dynamic friction coefficient between tire and compacted asphalt mixtures using tire-pavement dynamic friction analyzer. Construction and Building Materials, 258, 119492.

Zhang, S.W. (2004). Tribology of Elastomer, Tribology and Interface Engineering Series, 1st Edition, Elsevier, Amsterdam.